Chemometrics and Intelligent Laboratory Systems 193 (2019) 103847

Contents lists available at ScienceDirect

Chemometrics and Intelligent Laboratory Systems

journal homepage: www.elsevier.com/locate/chemometrics

Image analytical sandstone plug poro-perm prediction using angle measure technique (AMT) and chemometrics – A feasibility study

Maths Halstensen [a,*], Knut Kvaal [b], Kim H. Esbensen [c,a,d]

[a] University of South-Eastern Norway, Porsgrunn, Norway
[b] Norwegian University of Life Sciences (NMBU), Aas, Norway
[c] KHE Consulting, Copenhagen, Denmark
[d] Geological Survey of Denmark and Greenland (GEUS), Copenhagen, Denmark

A R T I C L E I N F O

Keywords:
Poro-perm
Image texture analysis
Angle measure technique (AMT)
Partial least squares regression (PLS-R)
Sand stone
Drill core plug

A B S T R A C T

This feasibility study evaluates an approach for prediction of sandstone plug porosity and permeability based on low-angle illumination imaging, the Angle Measure Technique (AMT) and chemometric multivariate calibration/validation. The AMT approach transforms 2-D texture images of drill core plug ends into 1-D 'complexity spectra' in which inherent porosity- and permeability-correlated features are subsequently extracted and subjected to multivariate calibration modelling. A training data set was selected because of its wide-spanning porosity and permeability ranges allowing evaluation of realistic prediction performance for typical North Sea/Scandinavian sandstone oil/gas reservoir rocks. This first study makes use of sand stone plugs from a single drill core from the Danish underground. Contingent upon proper test set validation (deliberately not deleting a few small, potential outliers), prediction performance assessment were for porosity [%] slope: 0.86; RMSEP: 2.2%; $R^2 = 0.90$ and for permeability [mDarcy]: slope: 0.91; RMSEP: 458 mDarcy; $R^2 = 0.87$, which translates into $RMSEP_{rel}$ of 12% and 19% respectively. These results pertain to a typical, well-spanning training data set (18 sandstone plugs); it is therefore concluded that the AMT approach to poro-perm prediction from images is feasible, but further, extended calibrations must be based on a more comprehensive training data sets covering the full geological regime of reservoir sandstones. We discuss possible application potentials and limitations of this approach.

1. Introduction

The present project is a feasibility study of the possibilities, and constraints, of a method for prediction of porosity and permeability from images of routine sandstone drill core plugs as used intensively in the oil/gas industry for physical measurements. This approach, if properly validated and accepted, *could* for example find use as a screening complement to such routine poro-perm determination in the core laboratory a.o.

The present feasibility study is only directed towards outlining if, and if so, to which degree it is possible to predict sandstone porosity and permeability based on texture image analysis in the form of AMT, combined with multivariate calibration PLS-regression. The perfunctory test set validation used allowed estimation of a realistic prediction error for both sandstone parameters. This is not an optimization study directed at comparing alternative image analytical texture transforms, of which one could find many e.g. Grey Level Co-Occurrence Matrix (GLCM), Wavelet Texture Analysis (WTA). It was found prudent to resolve the basic feasibility objective first. The results reported here are not likely to be the final optimal characteristics, so much interesting follow-up work can be expected.

Solymar and Fabricius [1] and Cipolloni et al. [2] have previously shown that porosity and permeability can be determined using classical image analysis and statistics. Coskun & Wardlaw [3,4] proposed an empirical image analytical method which describes how porosity and permeability influences water saturation in sand stone core plugs. The results indicate that the increasing volume of well-connected pores and increase in pore size uniformity improve recovery efficiency. James [5] showed that petrographic image analysis was suitable for characterization of fluid-flow pathways in a sand stone reservoir. His findings showed how the porous microstructure of a reservoir can explain the dynamic flow behavior in and around a production well.

The Angle Measure Technique (AMT) was introduced in 1994 by Robert Andrle [6] as a new method for characterising geomorphic lines

* Corresponding author. University of South-Eastern Norway, Kjolnes Ring 56, N-3918, Porsgrunn, Norway.
E-mail address: maths.halstensen@usn.no (M. Halstensen).

https://doi.org/10.1016/j.chemolab.2019.103847
Received 5 March 2019; Received in revised form 11 September 2019; Accepted 12 September 2019
Available online 14 September 2019

where relevant 'complexity features' are extracted as a function of a scaling parameter S. In 1996 Esbensen et al. [7] introduced the AMT approach in a broader generic sense as a promising method also in many technological applications. By combining AMT with chemometrics, they showed the potential of AMT for *texture analysis* in images. Kvaal et al. [8] compared five feature extraction techniques for characterisation of sensory porosity from texture images of bread; singular value decomposition SVD, auto-correlation and auto-covariance functions ACF and the so-called size and distance distribution SDD. In this study bread was used as a stand in proxy for many other types of materials with a characteristic pore void/matrix texture with a perhaps more significant impact in science, technology and industry. It was concluded that AMT was the best method for extracting sensory-related porosity measures from images.

From the beginning in the mid-1990's, multiple research projects based on the AMT method have subsequently been conducted and reported.

A significant number of publications have focused on method development and improvement of the angle measure technique [6–8,11,15,16,19,20]. A software package for AMT has been implemented in recent years and is available upon request [15]. The application areas of AMT span from powder technological particle characteristics such as porosity, size, shape etc. [7–10,12,14] to medicine [13], food science [7,8,17,21] and forensic studies [18,23]. The latest evaluation of AMT in a waste water treatment plant study has shown that the use of AMT in optimization of coagulants is a highly relevant method [22].

Esbensen et al. [7] and Kvaal et al. [8] applied multivariate modelling of AMT spectra of texture images and it was concluded that AMT was successful to extract relevant features for reliable prediction of porosity. AMT for quantification of permeability was proposed by Huang et al. [10] where AMT was applied to images of powder to quantify various bulk powder properties. However, it was concluded that it was not possible to predict permeability of the food related powders investigated in that study.

On this basis it was decided to *attempt* the rather ambitious goal of predicting both porosity as well as permeability of oil/gas reservoir sand stone plugs directly from digital images, for example as obtained during routine core slab photo documentation. This approach is contingent upon seamless interaction between digital imaging (with optimised low-angle

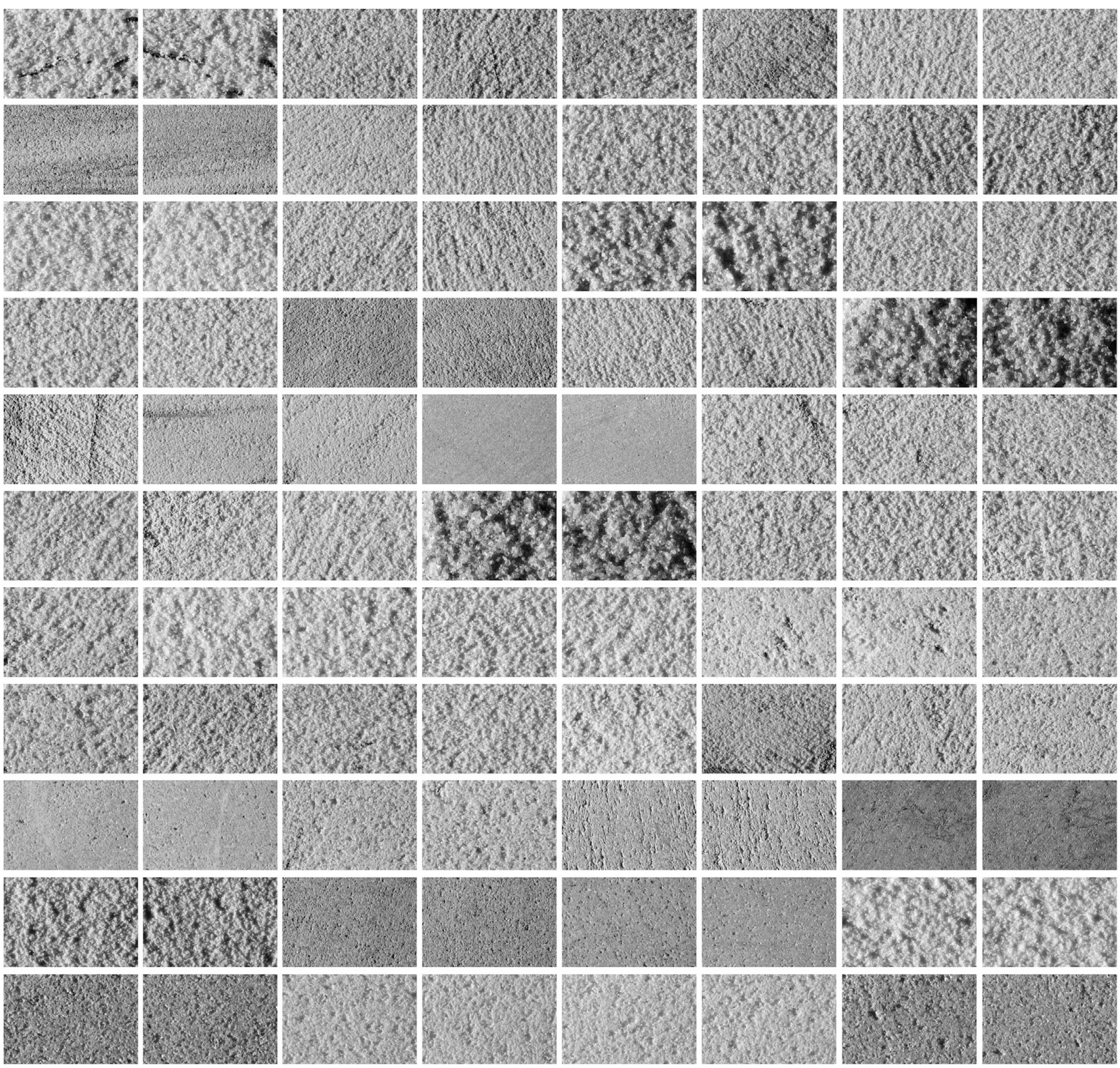

Fig. 1. Calibration and validation sandstone plug images obtained according to the unilateral low-angle illumination imaging described in the text. Each plug is represented by two juxtaposed images [cal; val], also further described in the text and in Fig. 3. Observe the visually successful span obtained from fine-grained to coarse-grained sandstones. The present feasibility study attempts to model the quantitative range of poro-perm related image features using the AMT transform. Individual horizontal image edge: = 23 mm.

illumination), the AMT 2-D to 1-D transformation and chemometric data modelling. The following reports on this feasibility study.

2. Materials and methods

2.1. Sand stone core plugs

A typical sandstone plug set was obtained from the public parts of GEUS′ extensive national drill core archive. Sandstone core plugs were selected and screened from the open access 'Helsingborg drill core', using in-house core laboratory porosity and permeability data. The sandstone facies of this core is known to correlate with typical reservoir sandstone in the Danish North Sea oil and gas province [24,25]. While most other aspects of the test results obtained from this drill core are proprietary, GEUS permitted use of the plug results obtained in GEUS core laboratory, used here as porosity and permeability reference determinations [26]. The plugs had previously been cleaned according to standard procedures at GEUS' core lab.

The primary criterion for inclusion was the quantitative span with respect to porosity, as revealed by the training data set depicted in Fig. 1. This figure illustrates well the unilateral low-angle illumination 'light/shadow' rendition of the sandstone plug end appearances which is the basis for the subsequent AMT transform, described below. One observes only a very few, if any, examples of residual cutting traces from the diamond saw used for plug production in this data set, in which great care was taken to acquire only the best quality plug end cuts.

2.2. Camera rig

It was considered as a welcome challenge to conduct this feasibility study with a minimum of equipment costs. The experimental setup used for image acquisition consists of a standard camera stand with a vertically mounted camera, focusing on sandstone plug end surfaces, see Fig. 2. The camera focal length distance (standard, high-level digital camera) is adjustable vertically to allow for varying plug lengths. A high-quality video projector was used for the illumination source because of the high luminous intensity and the even distribution of light on the plug surface. The angle between the plug surface and the illumination axis is adjustable for angle optimization, α, which has previously been shown to be an application-dependent success factor [7–11,14]. The technical specification of the image acquisition facility is listed in Table 1, which also report the camera settings used image acquisition of all plugs investigated in this study. From this context it is clear that the most critical success-factor is the camera resolution. For the purpose of the present feasibility study, a camera with 18 megapixel resolution was considered satisfactory.

Fig. 3 shows the pertinent details of the imaging approach. It is particularly relevant to use opposite ends of the plugs selected as basis for

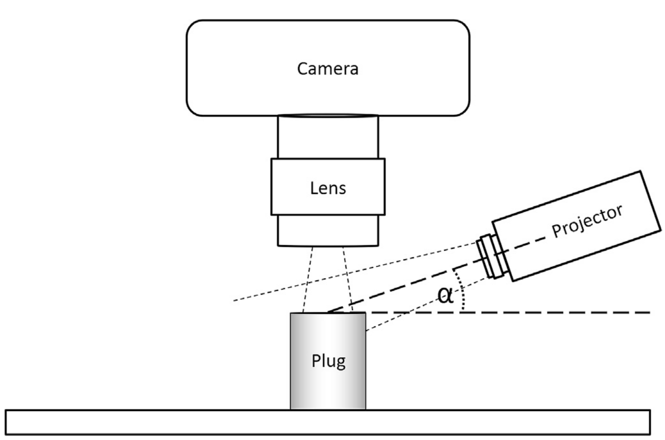

Fig. 2. Experimental camera rig (principal sketch).

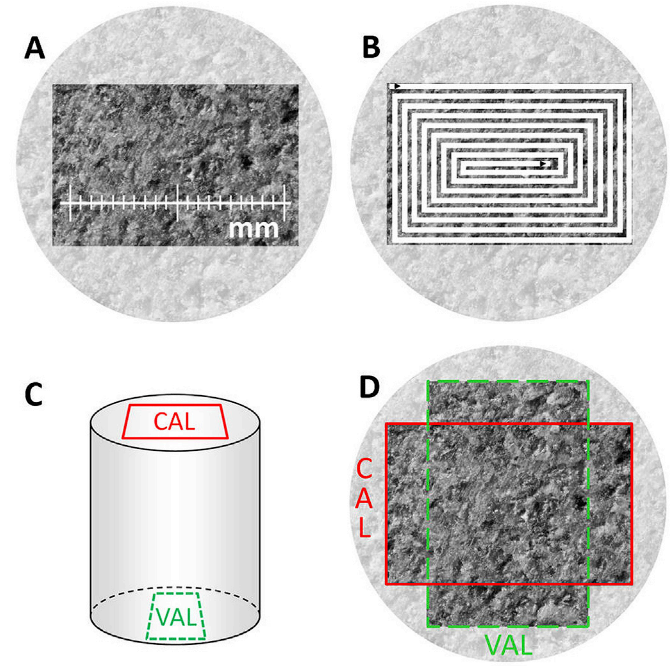

Fig. 3. Sand stone plug imaging. A: mm scale, B: spiral unfolding scheme, C: calibration and validation images from top and bottom of plugs, D: calibration and validation image orientations. The low-angle illumination (12°) light/shadow photographic details are especially well illustrated in A) and D).

Table 1
Technical specification of camera rig.

Camera:	Canon EOS 100D
Shutter time:	1/25 s
Aperture:	F/14
ISO:	200
Resolution:	18 megapixels
Lens:	Canon MP-E 65 mm 1–5x Macro Lens
Magnification:	1–5x
Focal length:	65 mm
Illumination projector:	Acer X112 DLP projector
Illumination angle α:	12° [see refs 7–10,14]
Camera stand:	HAMA Repro table

calibration and validation images, since these end-faces bracket the cylindrical plug volume through which permeability measurements have been conducted. It is equally relevant to estimate the porosity from the images of each plug end in order to force an element of practical relevance into a test set validation context.

From the results and experiences covering several AMT development studies, it is important how low-angle illuminated 2-D texture images are *unfolded* to become a 1-D feature vector [7–11,14]. It was found in Ref. [11] that the *spiral unfolding* scheme had many advantages, and this approach was also used here; see Refs. [7,11,14] for more in-depth discussion of the unfolding issue.

3. Experimental

3.1. Image analysis

Digital photos of plug end surfaces were obtained under the camera settings reported in Table 1. Image width = 23 mm and the resolution (mm/pixel) is 2.7 μm. Since the length of the selected sandstone plug varied significantly, the camera was traversed vertically until plug surfaces was in focus, to ensure that camera, focus and lens settings were *identical* for all images acquired. The physical length corresponding to one pixel width must be identical for all images (plugs) since their derived AMT spectra (see below) furnishes the basis for a multivariate calibration (*X*-data). The illumination source was also adjusted according to the height of the plugs to ensure that the illumination angle was identical, 12°, for all images (there is a curious analogy with a quite different matter[1]).

3.2. Training and test set selection

It was decided to use the one end of each plug (selected randomly) as part of a chemometric *training data set* (see further below), with the opposite end forming a bona fide *test set*, Fig. 3. The distance between plug ends spans a few centimeters (plugs are sub-drilled with their longitudinal axis corresponding to the horizontal sedimentary rock formation bedding direction), thus allowing the pertinent *local* along-bedding heterogeneity to play a role commensurate with the reference laboratory poro-perm measurement scale, cfr. Fig. 3c, see Halvorsen and Hurst (1990) for details concerning relevant permeability measurement setups [27]. Fig. 3c and d shows how this disposition was realised. From a data analytical point of view this setup constitute a meaningful and realistic training vs. test set according to the 'principles of proper validation' laid out in Esbensen & Geladi (2010) [28] and Esbensen & Swarbrick (2018) [29].

3.3. Data set prequalification

Fig. 4 shows a typical permeability vs. porosity plot, which is a standard feature in all oil/gas reservoir rock characterisation projects. There is often a medium-to-strong correlation relationship between these two parameters, but not over all ranges.

From Fig. 4 it is apparent that sandstones with effective porosities below 15% behave markedly different from all other plugs in the set used here. From general background knowledge pertaining to the geology of the Helsingborg drill core, it is likely that porosity tapers off dramatically below this threshold due to secondary precipitation in the porous voids, effectively closing the 3-D void network, also, in particular, as regards flow-through possibilities.

This relationship notwithstanding, it was decided to keep these plugs, at least in a first modelling step, to see whether it would be possible to model porosity and permeability separately, perhaps including these apparently deviating data. If this turned out not to be the case, deletion of these low poro-perm rocks would be quite acceptable, as the goal of sandstone poro-perm prediction of course is only directed at typical and realistic void and flow regimes of relevance for the oil and gas industry, which is precisely above 15% porosity.

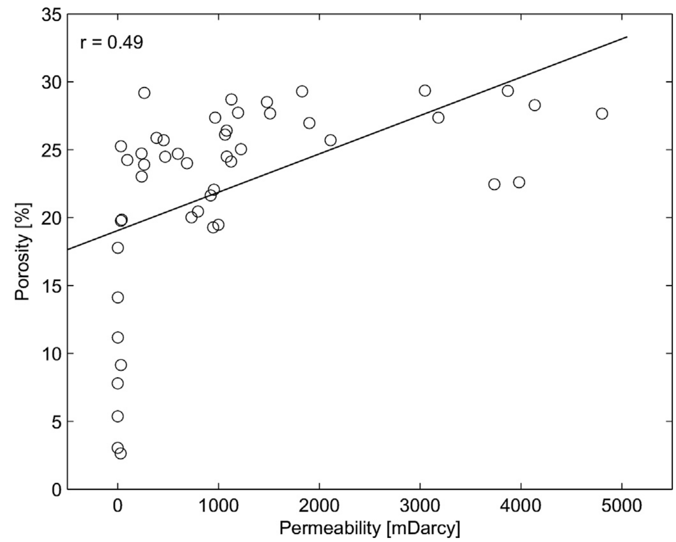

Fig. 4. Permeability [mDarcy] vs. Porosity [%]. Porosities below 15% could be excluded from the training and test data sets, but were retained in the modelling in this project, see text for details.

3.4. AMT – image pre-processing

The AMT transform operates on data organised as 1-D measurement series, either original data types (e.g. time series) or other types of data which have been transformed into such a format, in the present case *unfolded* digital 2-D texture images, as illustrated in Fig. 3b here using a spiral unfolding vectorisation. Original as well as transformed 1-D data series can be subjected to the Angle Measure Transform (AMT) according to the detailed descriptions found in Refs. [6–8]. Suffice with the briefest phenomenological introduction here, see Fig. 5.

The unfolding issue revolves around alternative ways to linearise ('vectorise') a digital image, for which there are three principal alternatives, colloquially termed "chop-chop", "snake" and "spiral". These should only be applied to images of an isotropic nature i.e. not dominated by anisotropic structural elements or marked periodic patterns, but are well suited for unfolding of texture images like the ones presented in this paper. Based on decades of experience some effects related to the specific

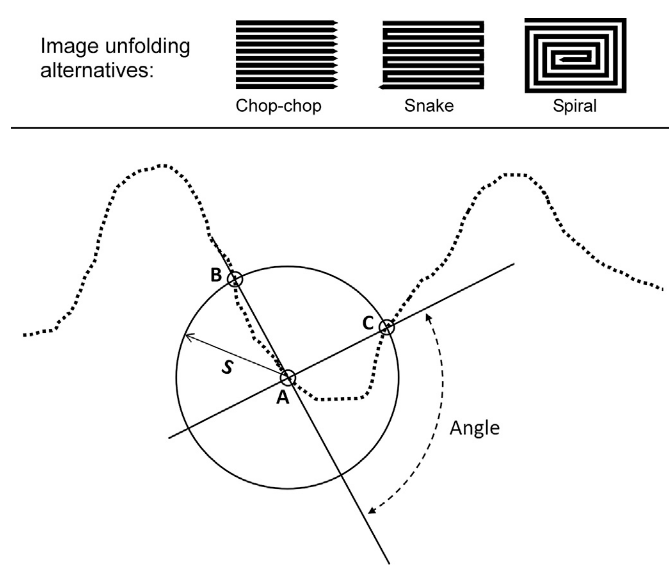

Fig. 5. Top: Image unfolding alternatives. Bottom: The elements in the Angle Measure Technique (AMT) [1,11]. Point A is a randomly selected datum from the full unfolded data series.

[1] In the year of the 50th anniversary of the first Moon landing, it is interesting to note that the exact same topic had also been the subject of quite intense study, albeit in an apparently completely different context: *"Now that Armstrong was headed beyond the crater, he needed to pick a good spot to land, a potentially difficult enterprise given the very peculiar lighting conditions affecting the Moon's surface which there had been no way to simulate on Earth. 'It was of great concern' recalled Neil Armstrong, 'that as we got close to the Moon, the reflected light off the surface would be so strong, no matter what angle we came in on, that a lot of our vision would be wiped out, seriously affecting our depth perception.' Fortunately, NASA's mission planners had given plenty of forethought to the photometrics involved. They had concluded that, for optimum depth perception, the Eagle (the Lunar Excursion Module, LEM) needed to land at a time of "day" and at an angle that produced the longest possible shadows. Where there were no shadows, the Moon looked flat, but where shadows were long, the Moon looked fully three-dimensional. […. .] The ideal condition occurred for the descent trajectory of the LEM when the Sun was* ***12.5 degrees above the horizon****. That was the time when Neil Armstrong and Buzz Aldrin would have adequate light over the landing area and still strong depth-of-field definition."* Quotation from p. 248 in James R. Hansen (2018) "FIRST MAN – The Life of Neil Armstrong" 3.rd ed. Simon & Schuster. ISBN 978-1-9821-0316-3 (emphasis, present authors) [30].

choice of unfolding approaches have come to light.

Chop-chop unfolding: an artifact, a discontinuity along the unfolded dimension is introduced (with a period corresponding to the image width) which is a reflection of different texture pixel patterns at the two edges of the image, which may be of varied magnitude. This translates into a (minor, major) periodicity artifact in the AMT spectra.

Snake unfolding: dampens this discontinuity effect, but will result in a near-field 'shadow correlation' between pixels along two, close-lying consecutive digital image lines with regular occurrences.

Spiral unfolding: will only result in such correlation effects between pixels along a few image lines in the center of the image.

The side effects of the two latter methods are reduced significantly by selection of random AMT center pixels on the unfolded digitized line. The artifact from Chop-chop is by far the most prominent, for which reason Chop-chop is no longer used. As the Spiral method only has unwanted effects in the narrow center of the spiral pattern, a minute fraction of the total line distance - which routinely is deselected in practical use, this approach is superior. It is fair to relate however, that in practice Spiral and Snake often produce very comparable unfolded 1-D versions of texture images.

A number (n) of points, A, (2500 points) on the unfolded intensity curve are randomly selected from the entire data series (using a stratified random selection option, 20 segments (strata). Stratification is the process of dividing the members of the population into homogeneous subgroups prior to sampling. Then, single random sampling or systematic sampling within each layer is used. The goal is to improve the precision of the sample by reducing the sampling error. For each point A_n a circle with a radius with the contemporary scale (s) is drawn. The circle intersect the intensity curve at two points B_n and C_n The supplementary angle of $C_nA_nB_n(s)$ is calculated for all sample points n. The average value of all $C_nA_nB_n(s)$ is then calculated, as MA(s) for the given s (Mean Angle). The scale s is then allowed to be incrementally raised to $s+1$, so that s ranges from 1 (minimum length $s = 1$ pixel) to a maximum value s_{max}, after which the MA process is repeated for each scale s up to s_{max}. The MA(s) values can be represented in a graph where the computed MA(s) is plotted as a function of the scale s; the resulting plotted line is the so-called AMT spectrum (Complexity Spectrum) as shown in Fig. 6.

The 88 final (44 calibration/validation) images used in this study were all subjected to an identical AMT transform as described above, which resulted in the set of Mean Angle (MA) complexity spectra displayed in Fig. 6. The X-matrix used for calibration of the models were 44 spectra and 500 variables (44 MA spectra and $s = 1$–500). The validation

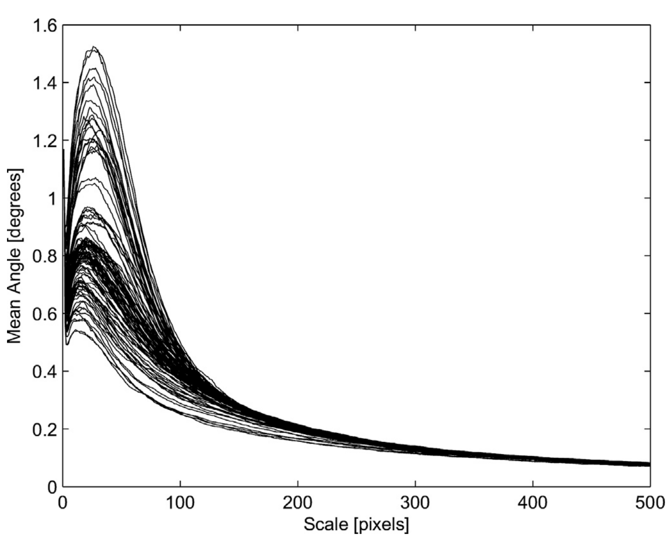

Fig. 6. Mean Angle (MA) spectra of all 88 sandstone plug images comprising the training + test set in the PLS-modelling below. These spectra can conveniently be collected into an X-matrix with a view of subsequent multivariate calibration.

data had identical dimensions.

3.5. PLS-R (method description)

Partial Least Squares Regression is an empirical -data driven -modelling approach which is well explained in literature [28,29] and therefore not explained in detail here. PLS-R relies on representative training data for two variable blocks, often called X and Y respectively. In the present study the X data matrix contains the mean angles for each scale parameter s, and Y is a vector containing the parameter of interest which is porosity or permeability since these are modelled separately.

4. Analysis & results

Figs. 7 and 8 show the complete PLS-R test set validation results for porosity and permeability individually, both models using 4 PLS-components.

4.1. PLS-R model relationships and interpretation

Although both models are supported by four components when test set validated, we only interpret and illustrate the first and second PLS-components here, because these account for the dominant >95% of the y-variable variance explained. The relationships described below will not change in any significant way were the PLS-models based on three, or two PLS-components.

The X-axis along which the X-variables are plotted represent *scale*. The 'ordering distance' from variable i to variable $i+1$ is physically identical to the unit pixel resolution, i.e. physically corresponding to a fraction of a mm as realised by the camera setup geometry, cfr. Fig. 2. Thus the variable identification number along the X-axis of the loading-weight plot in Figs. 7 and 8 corresponds to larger and larger physical scales. For both models, the total number of scale units used are 500, *ibid*. Thus it is easy to interpret the loading-weights (w-spectra) and to compare their scale significance. Interpretation of both the original MA spectra as well as loading (p) or loading-weight (w) spectra, follows standard chemometric data modelling principles [29]. Thus one, or more, prominent scale mode(s) (peaks) represent a dominant scale that is strongly involved in supporting the data analytical model [6–14,29]. delved into these interpretation matters in full detail regarding a suite of quite different y-variable types that all could be related to the specifics of the suite of MA spectra collected into a data analytical X-matrix.

For the present PLS-models, the interpretation of the w-spectra is easy and clear. The w_1 spectrum reveals a prominent uni-modal peak corresponding to a scale of ~25 pixels for both the porosity and the permeability model. This scale physically corresponds to ~67.5 μm, representing the average size of the geometric light/shadow elements of all the samples included in the training data set. This is either the average grain size and/or the average void size, which are highly correlated because of the low-angle illumination producing the light/shadow photos. This means that the t_1-score of a particular sample is *proportional* to the average pore size of this sample – a smaller or larger t_1-score corresponds to smaller or larger average pore sizes of the suite of samples studied. This is strongly corroborated by the special visualization plot pairs prepared as Figs. 9 and 10. Thus the first PLS-component in both models *represent* average pore size of the area shown in each original image. The major gamble in the present study is whether there also is embedded information in this type of light/shadow photos related to permeability, i.e. whether a PLS model can also extract information upon which a permeability model can be constructed.

From Figs. 7 and 8, which overall show a markedly similar w-loading weight pattern, it is clear that the basis for the present separate models for porosity and permeability, owes a lot to the internal strong correlations between these two parameters, cfr. Fig. 4.

In this context, the patterns modelled by the second PLS-components in both models are of particular interest. Both reveal a bi-modal,

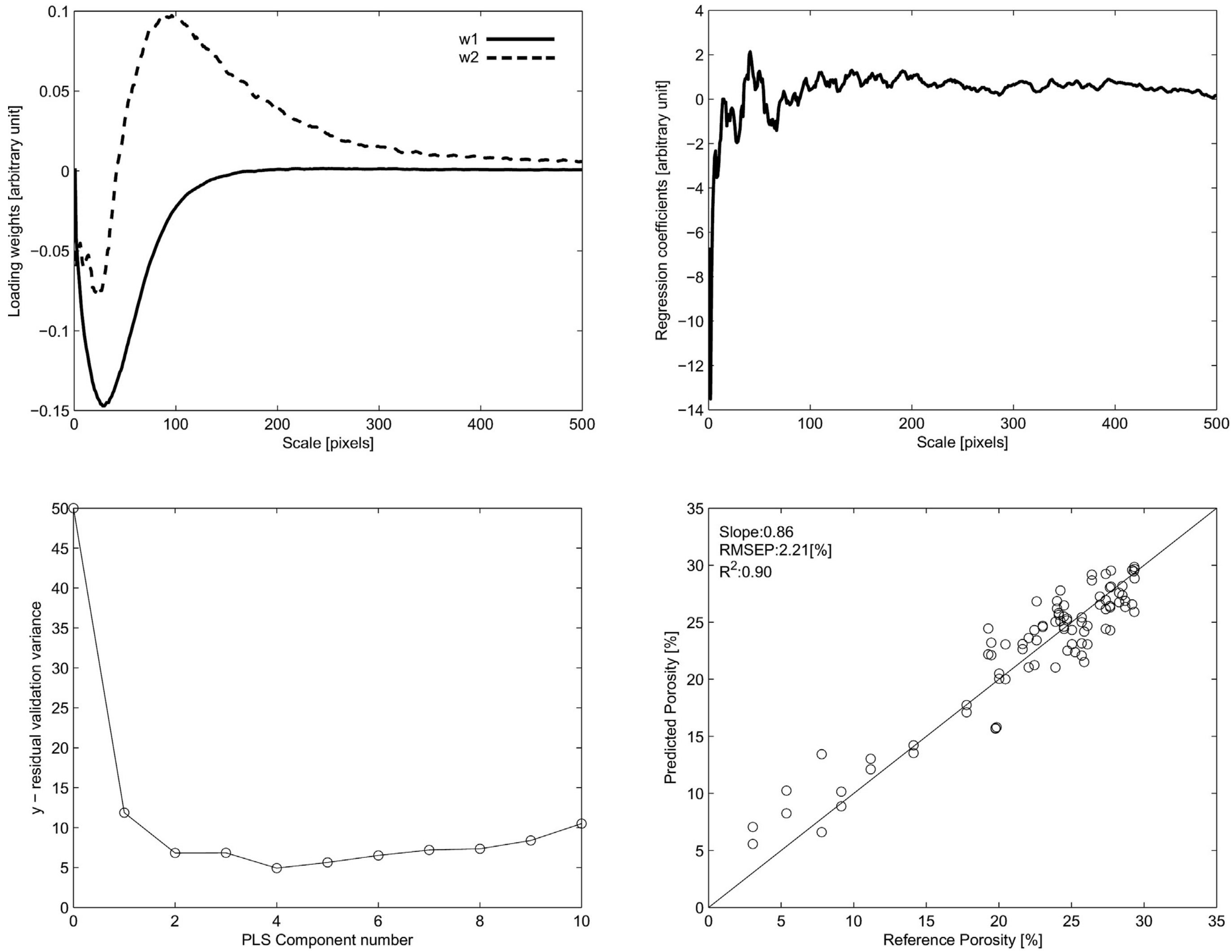

Fig. 7. PLS-R modelling and validation results when prediction sandstone plug porosity [%]. Test set validation parameters, slope: 0.86; RMSEP: 2.2% ($RMSE_{cal}$: 2.08%); $R^2 = 0.90$. The optimal PLS-model used 4 components. $RMSEP_{rel} = 12\%$.

antithetic pattern with a first mode slightly smaller than for the w_1-spectra, which is anti-correlated with a second, larger scale mode. This overall pattern is generally in common for both PLS-models, although different with respect to minor details between the porosity and the permeability models. Careful scrutiny of the special visualization plots presented below in which the original texture images are included, indicate that the second PLS-component models a partially different physical aspect than the first. More detailed physical interpretations are best postponed until a more comprehensive data set is available. It is clear that what *might* work for one specific realization of reservoir rock sandstones, certainly must also be thoroughly tested against other reservoir sandstones in a geologically well bracketed design.

Figs. 9 and 10 illustrate details of the relationships between the visual texture images and their internal relationships in the models, the latter as revealed by t_1-t_2 score plots from the individual PLS-regression models. There is a regular gradual relationship between image texture features and the disposition of the plug samples in the score plots.

The perhaps most remarkable feature is that it turns out to be fully possible to *include* the <15% porosity samples identified in Fig. 4 in the porosity model – while these samples serve only to “smear out” the effective zero level for permeability; they may better be deleted here. These relationships are shown with clarity in the ‘predicted vs. reference’ plots in Figs. 9 and 10.

4.2. Validation

This feasibility study makes use of test set validation [28,29], for which reason the quoted validation statistics are reliable characteristics of the prediction performances for porosity and permeability for *similar* sandstone rocks, but in this feasibility study all rocks derive from the same depth interval in one drill core only.

Figs. 9 and 10 are presented for additional insight into the merit and validity of the training and test set definition chosen. In these plots the calibration image and the corresponding test set image renditions are identified by a ‘connecting line’. This allows visual appreciation of the degree of similarity/dissimilarity between corresponding pairs of plug ends; it especially allows identification of *pairs of relatively marked dissimilarity*, of which each plot contains ~3–5. It is observed that these pairs are not the same for porosity and permeability respectively, attesting to different 3-D void/matrix and pore connectivity relationships in some of the individual rocks involved [27]. These discrepancies may also relate to different degrees of residual cutting traces left on opposite ends for a small number of plugs.

For the feasibility study purpose it suffices to acknowledge that such larger-then-average calibration-validation image differences constitute the most influential components in the RMSEP levels achieved, i.e. in cases where the one plug end is revealed to be more different from the

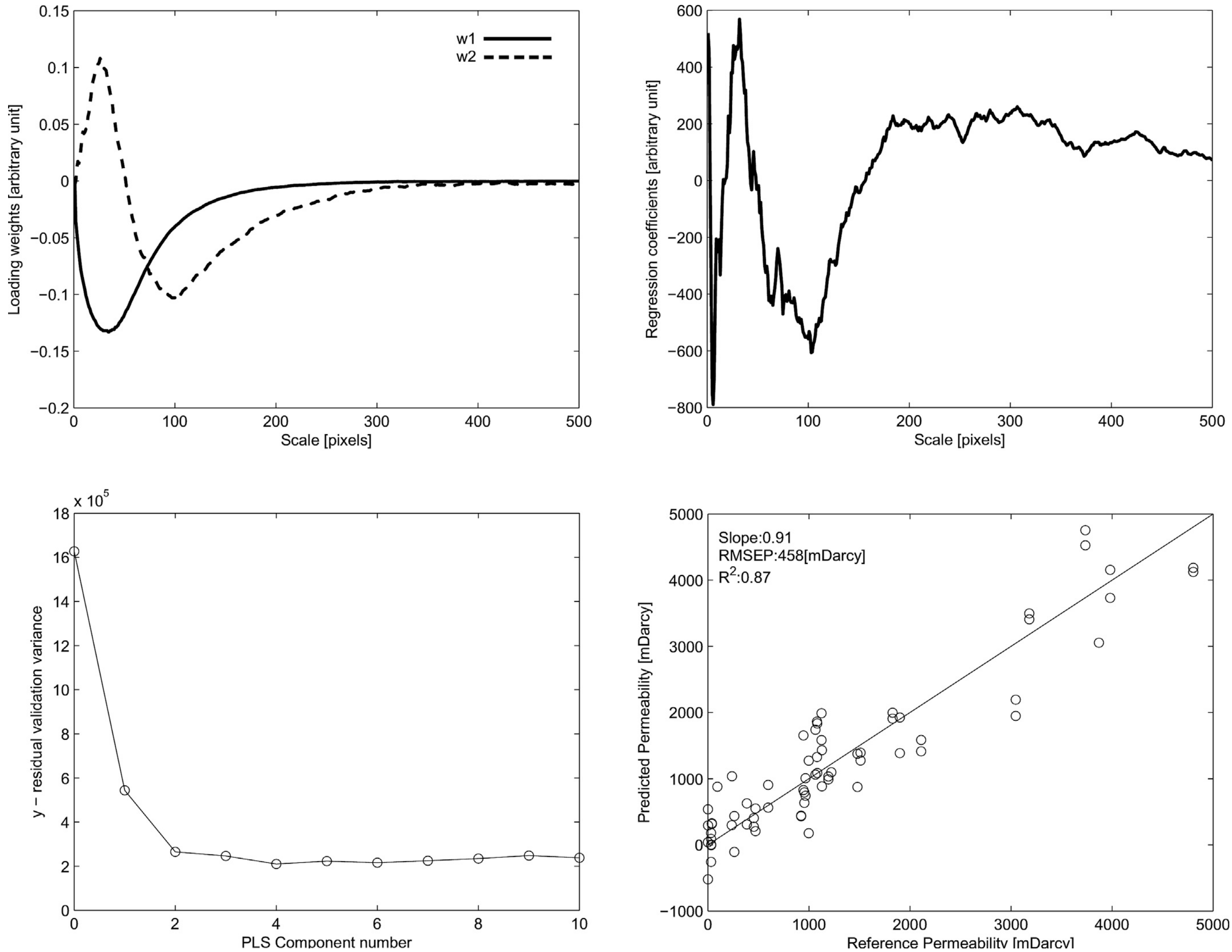

Fig. 8. PLS-R modelling and validation results when predicting sandstone plug permeability [mDarcy]. Test set validation parameters, slope: 0.91; RMSEP: 458 mDarcy ($RMSE_{cal}$: 372 mDarcy); $R^2 = 0.87$. The optimal PLS model uses 4 components. $RMSEP_{rel} = 19\%$.

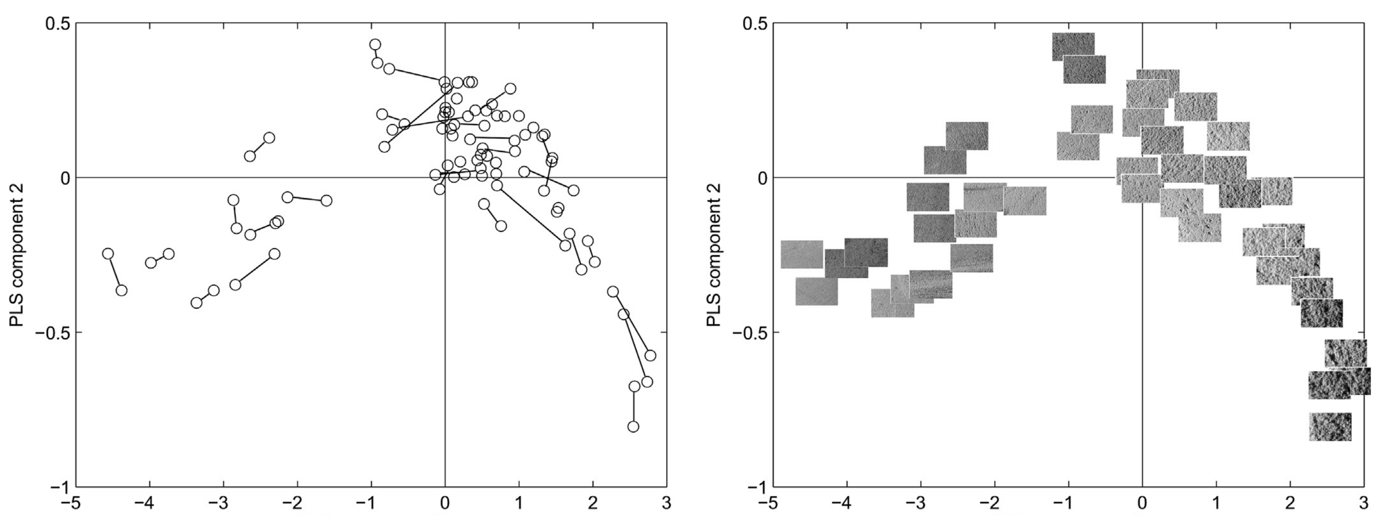

Fig. 9. Left: Score plot t1-t2 for the PLS-R model of porosity [%] Calibration and validation images connected with lines. Right: Score plot t1-t2 for the PLS-R model of porosity [%] with selected plug images.

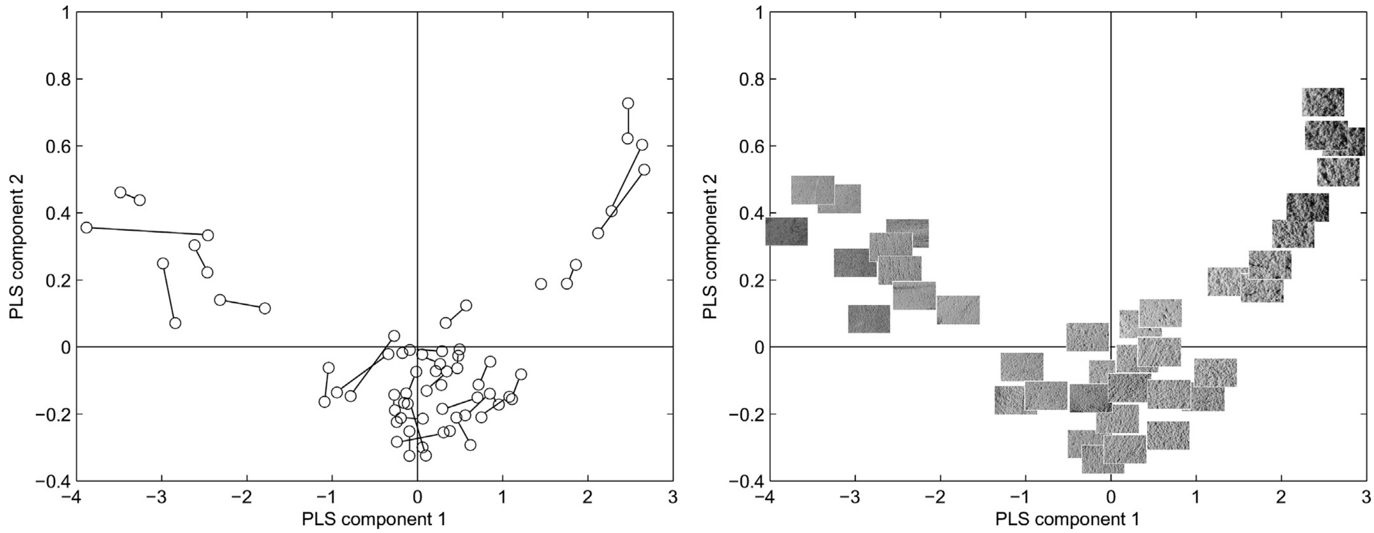

Fig. 10. Left: Score plot t1-t2 for the PLS-R model of permeability [mDarcy] Calibration and validation images connected with lines. Right: Score plot t1-t2 for the PLS-R model of permeability [mDarcy] with selected plug images.

other compared with most other plugs in the data set, this local scale heterogeneity makes a larger-than-average contribution to the overall prediction uncertainty, i.e. will inflate RMSEP to some degree, which would not be the case were these samples deleted as outliers. There is nothing here that is not as expected on general grounds considering the geology of sedimentary sandstone rock in general; see for example [27]. It has here been decided not to carry out such outlier policing in order to subject the feasibility study testing to the most stringent conditions.

This kind of plot allows insight into plug heterogeneity *per se* and partly also to larger scales in oil/gas reservoirs, to the degree that the full plug set selected is representative for this regimen. The issue of individual plug representativity w.r.t. the drill core from which there have been extracted is a topic for further discussions in the geological realm.

A specific variant of RMSEP validation parameter, suitable for comparison, is the relative $RMSEP_{rel}$ measure, defined as RMSEP x 100 [%]/average laboratory level. For porosity and permeability $RMSEP_{rel}$ comes to 12% and 19% respectively, which is deemed as a *fair* prediction performance statistics for a very first feasibility study. For comparison the analytical uncertainty of reference measurements (GEUS core laboratory) for porosity at 95% level of confidence (± 2 std) is 0.2 p.u. (%). For permeability the analytical uncertainty is declared to be in the interval 6–15%(rel) (high-to-low permeability).

The degree of confidence one can assign to such first precision level estimates depends entirely on the representativity of the single drill core used in this study. It was decided to do a first feasibility study based on one well, carefully selected, simply to be able to progress to a significantly more elaborated training/test set on a reasonable 'proven basis' - or to terminate this image analytical approach at this stage. Thus there are several features of the calibration/test sets that indeed are open for potential considerable improvement(s), e.g. it is highly desirable with plugs from more than one (preferentially many, well selected) randomly selected well commensurate with the relevant type(s) of reservoir sandstone formations, and of course the obligatory data modelling comment wishing for a larger training set, i.e. more training set plugs. While the low-angle illumination was mainly fixed based on earlier studies, the specific value of 12° w.r.t. horizontal would not appear to be a candidate for significant improvements, given the somewhat broad target material types discussed in the introduction (see also footnote 1).

5. Conclusions

A new approach for prediction of porosity and permeability in sandstone drill core plugs using AMT transformed images and chemometric multivariate calibration PLS models has been feasibility tested. Based on a single drill core from the Danish underground carrying a realistic span of both porosity and permeability levels for typical of oil and gas field sedimentary sandstones, which furthered a reasonable number of initial plug samples, stringent test set validation (deliberately not involving outlier policing), revealed a first estimate of prediction performance corresponding to $RMSEP_{rel}$ of 12% and 19% for porosity and permeability respectively. These are considered fair and satisfactory feasibility study results.

From general geological understandings there would appear to be good reasons to expect a possible significant lowering of these estimates when a more comprehensive set of relevant plugs is available for a full-scale technological calibration. In this context, a comprehensive oil & gas reservoir geology competence and experience will be *the* critical success factor for possible improved modelling and prediction ability.

6. Perspectives

Within the oil/gas industry sector, since 1990 there has been a gradual phasing in of *mini-permeametry* as a complement to traditional Hasler-sleeve laboratory method, the results of which are still considered authoritative. But this comes at the price of a significantly larger effort and cost outlay. This development was first described in 1990 [27], who then predicted a time at which a well-calibrated and extensively tested mini-permeametry regimen *might*, if not completely have taken over, then certainly fulfill a role as a full-fledged *complementary* approach because it allows a considerable higher number of determinations at the same accuracy and precision levels.

The present, still more effortless and considerably more effective approach, was originally conceived as but one extension along the lines of several other studies involving the new AMT transform and its potential induction into technology and industry sectors. Several of the previous AMT studies discussed in the introduction also employ the scope of the 2-D image-to-vector unfolding precursor to AMT complexity characterization, but the specific application to porous media has long only been a "what if" possible option by the senior author (KHE), earlier pioneered by application to aggregate media in the scale regimens of powders, sand and similar materials.

With the present feasibility results there *may* emerge an analogue development as became the fate of mini-permeametry. However, there are also valid grounds for not overstating this potential. This is so because all chemometric multivariate calibration models, to be used for extremely efficient prediction, are *empirical* and always critically dependent upon the availability, validity and representativity of the training and test sets involved. The powerful prediction potential of well calibrated PLS-models must at all times be checked by proper empirical validation, i.e. test set validation [28,29] in the most realistic contexts possible.

So, there is a way to go still, applying the present IA-AMT-PLS approach to many more relevant training/validation data sets of close relevance to the many geological specifics pertaining to oil/gas reservoir rocks in general and to individual sedimentary basins, before a fully tested facility can be said to have been established. As but a few, easily envisaged possible humps on the road forward, mentioning should be made of:

i) Only cleaned plugs are relevant for the present kind of imaging
ii) Only pristine porous/permeable reservoir rocks are relevant. There must be no significant void precipitations or metamorphic transformation of the original sedimentary rocks ‘closing up’ the interconnecting ‘necks’ connecting pore voids
iii) No significant cutting defects degrading the imaging quality of plug ends (no saw marks etc.) There *may* perhaps be secondary progress possibilities focusing on the specific diamond cutting procedures in use.
iv) It is fully possible to use a higher resolution camera which in all likelihood will be able to furnish a more detailed light/shadow rendition of the plug end details which may, or may not, be able to improve the modelling efficiency for the second (or higher) PLS-components?

However, should (all) such potential issues be successfully overcome, the only remaining roadblock would appear to be the quality and geological representativity of the training/validation sets. But these are all principally easy issues to resolve; there exist a plethora of already completed drill cores from all the world’s very many oil and gas fields, very many of which complete with plugs and relevant poro-perm data also available. The last troublesome issue would then be related to the considerable logistics concerning getting permission to collect the kind of “across-company” sample sets ultimately desired, but perhaps in-house or in-company samples will suffice for many purposes.

The present experimental approach, if/when properly further validated and accepted, *could* for example find use as a screening complement to more elaborate and workload demanding poro-perm determination in the core laboratory a.o.

Conflicts of interest

The authors have no competing interests to declare.

Acknowledgements

GEUS is thanked for permission to use the pertinent set of sandstone plugs derived from the open access ’Helsingborg drill core’. The authors are very grateful to the erstwhile GEUS core laboratory head over several decades, Mr. Niels Springer, for providing indispensable metrology insight and perspectives on current porosity and permeability measurement procedures which has influenced the thinking behind the present approach (2010–2015).

Appendix A. Supplementary data

Supplementary data to this article can be found online at https://doi.org/10.1016/j.chemolab.2019.103847.

References

[1] M. Solymar, I.L. Fabricius, Image analysis and estimation of porosity and permeability of arnager greensand, upper cretaceous, Denmark, Phys. Chem. Earth (A) 24 (No) (1999) 587–591.
[2] G. Cipolloni, C. Menapace, I. Cristofolini, A. Molinari, A quantitative characterization of porosity in a Cr-Mo sintered steel using image analysis, Mater. Char. 94 (2014) 58–68.
[3] S.B. Coskun, N.C. Wardlaw, Influence of pore geometry, porosity and permeability on initial water saturation-An empirical method for estimating initial water saturation by image analysis, J. Pet. Sci. Eng. 12 (1995) 295–308.
[4] S.B. Coskun, N.C. Wardlaw, Image analysis for estimating ultimate oil recovery efficiency by waterflooding for two sand stone reservoirs, J. Pet. Sci. Eng. 15 (1996) 237–250.
[5] R.A. James, Application of petrographic image analysis to the characterization of fluid flow pathways in a highly-cemented reservoir: Kane field, Pennsylvania, U.S.A, J. Pet. Sci. Eng. 13 (1995) 141–154.
[6] R. Andrle, The angle measure technique: a new method for characterizing the complexity of geomorphic lines, Math. Geol. 26 (1994) 83–97.
[7] K.H. Esbensen, K.H. Hjelmen, K. Kvaal, The AMT approach in chemometrics - First forays, J. Chemom. 10 (1996) 569–590.
[8] K. Kvaal, J.P. Wold, U.G. Indahl, P. Baardseth, T. Næs, Multivariate feature extraction from textural images of bread, Chemometr. Intell. Lab. Syst. 42 (1998) 141–158.
[9] J. Huang, K.H. Esbensen, Applications of Angle Measure Technique (AMT) in image analysis Part I. A new methodology for in situ powder characterization, Chemometr. Intell. Lab. Syst. 54 (2000) 1–19.
[10] J. Huang, K.H. Esbensen, Applications of AMT (Angle Measure Technique) in image analysis Part II: Prediction of powder functional properties and mixing components using Multivariate AMT Regression (MAR), Chemometr. Intell. Lab. Syst. 57 (2001) 37–56.
[11] P.P. Mortensen, K.H. Esbensen, Optimization of the Angle Measure Technique for image analytical sampling of particulate matter, Chemometr. Intell. Lab. Syst. 75 (2005) 219–229.
[12] J.B. Holm-Nielsen, C.K. Dahl, K.H. Esbensen, Representative sampling for process analytical characterization of heterogeneous bioslurry systems—a reference study of sampling issues in PAT, Chemometr. Intell. Lab. Syst. 83 (2006) 114–126.
[13] S. Kucheryavski, Using hard and soft models for classification of medical images, Chemometr. Intell. Lab. Syst. 88 (2007) 100–106.
[14] C.K. Dahl, K.H. Esbensen, Image analytical determination of particle size distribution characteristics of natural and industrial bulk aggregates, Chemometr. Intell. Lab. Syst. 89 (2007) 9–25.
[15] K. Kvaal, S.V. Kucheryavski, M. Halstensen, S. Kvaal, A.S. Flø, P. Minkkinen, K.H. Esbensen, eAMTexplorer: a software package for texture and signal characterization using Angle Measure Technique, J. Chemom. 22 (11–12) (2008) 717–721, https://doi.org/10.1002/cem.1160.
[16] S.V. Kucheryavski, K. Kvaal, M. Halstensen, P.P. Mortensen, C. Dahl, P. Minkkinen, K.H. Esbensen, Optimal corrections for digitization and quantification effects in angle measure technique (AMT) texture analysis, J. Chemom. 22 (11–12) (2008) 722–737, https://doi.org/10.1002/cem.1118.
[17] S.M.B. Johansen, J.L. Laugesen, T. Janhøj, R.H. Ipsen, M.B. Frøst, Prediction of sensory properties of low-fat yoghurt and cream cheese from surface images, Food Qual. Prefer. 19 (2008) 232–246.
[18] S. Kucheryavski, I. Belyaev, S. Fominykh, Estimation of age in forensic medicine using multivariate approach to image analysis, Chemometr. Intell. Lab. Syst. 97 (2009) 39–45.
[19] S. Kucheryavski, I. Belyaev, Classification and analysis of non-isotropic images by Angle Measure Technique (AMT) with contour unfolding, Anal. Chim. Acta 642 (Issue 1–2) (2009) 135–141.
[20] S. Kucheryavski, Extracting useful information from images, Chemometr. Intell. Lab. Syst. 108 (2011) 2–12.
[21] L. Fongaro, K. Kvaal, Surface texture characterization of an Italian pasta by means of univariate and multivariate feature extraction from their texture images, Food Res. Int. 51 (2013) 693–705.
[22] N. Sivchenko, K. Kvaal, H. Ratnaweera, Evaluation of image texture recognition techniques in application to wastewater coagulation, Cogent Engineering 3 (1) (2016) 1206679. http://doi.org/10.1080/23311916.2016.1206679.
[23] L. Fongaro, D.M.L. Ho, K. Kvaal, K. Mayer, V.V. Rondinella, Application of the angle measure technique as image texture analysis method for the identification of uranium ore concentrate samples: New perspective in nuclear forensics, Talanta (2016), https://doi.org/10.1016/j.talanta.2016.02.027.
[24] J. Andsbjerg, K. Dybkjær, Sequence stratigraphy of the Jurrasic of the Danish Central Graben, Geol. Surv. Den. Greenl. Bull. 1 (2003) 265–300.
[25] L.H. Nielsen, Late Triassic – Jurassic development of the Danish Basin and the Fennoscandian Border Zone, southern Scandinavia, Geol. Surv. Den. Greenl. Bull. 1 (2003) 459–526.
[26] Geological Survey of Denmark and Greenland (GEUS). http://www.eng.geus.dk/products-services-facilities/laboratories/core-laboratory/.
[27] C. Halvorsen, A. Hurst, Principles, Practice and Applications of Laboratory minipermeatry, in: P.F. Worthington (Ed.), Advances in Core Accuracy and Precision in Reserves Estimation, Gordon & Breach, 1990, pp. 521–549.
[28] K.H. Esbensen, P. Geladi, Principles of Proper Validation: use and abuse of re-sampling for validation, J. Chemom. 24 (2010) 168–187, https://doi.org/10.1002/cem.1310. www.interscience.wiley.com.
[29] K.H. Esbensen, B. Swarbrick, Multivariate Date Analysis – an Introduction to Multivariate Data Analysis, Process Analytical Technology and Quality by Design, 6.th edition, CAMO Software AS, 2018, ISBN 978-82-691104-0-1, p. 462.
[30] James R. Hansen, FIRST MAN – the Life of Neil Armstrong, 3.rd ed, Simon & Schuster, 2018, ISBN 978-1-9821-0316-3.